Mu Fan
State Key Laboratory of Mechanics and Control of Mechanical Structures,
Interdisciplinary Research Institute of Aeronautics and Astronautics,
Nanjing University of Aeronautics and Astronautics,
Room 217, Building A18, #29 Yu Dao Street,
Nanjing 210016, China
e-mail: mfanz@nuaa.edu.cn

Bolei Deng
StrucTronics and Control Lab,
School of Aeronautics and Astronautics,
Zhejiang University,
Hangzhou 310058, China
e-mail: dengbolei@zju.edu.cn

Hornsen Tzou
Fellow ASME
State Key Laboratory of Mechanics and Control of Mechanical Structures,
Interdisciplinary Research Institute of Aeronautics and Astronautics,
Nanjing University of Aeronautics and Astronautics,
Room 202, Building A18, #29 Yu Dao Street,
Nanjing 210016, China
e-mail: hstzou@nuaa.edu.cn

Dynamic Flexoelectric Actuation and Vibration Control of Beams

A flexoelectric cantilever beam actuated by the converse flexoelectric effect is evaluated and its analytical and experimental data are compared in this study. A line-electrode on the top beam surface and a bottom surface electrode are used to generate an electric field gradient in the beam, so that internal stresses can be induced and applied to distributed actuations. The dynamic control effectiveness of the beam is investigated with a mathematical model and is validated by laboratory experiments. Analyses show that the actuation stress induced by the converse flexoelectric effect is in the longitudinal direction and results in a bending control moment to the flexoelectric beam since the stress in the thickness is inhomogeneous. It is found that thinner line-electrode radius and thinner flexoelectric beam lead to larger control effects on the beam. The position of the line-electrode on the top surface of the beam also influences the control effect. When the line-electrode is close to the fixed end, it induces a larger tip displacement than that is close to the free end. Analytical results agree well with laboratory experimental data. This study of flexoelectric actuation and control provides a fundamental understanding of flexoelectric actuation mechanisms. [DOI: 10.1115/1.4039238]

Introduction

Cantilever beam model is among the most frequently used structures in engineering applications, such as wings, antennas, robot arms, etc. A systematic study on the dynamic control of a cantilever beam has been conducted by Soedel [1] and Qatu [2]. In last few decades, many studies of precise actuation and vibration control of cantilever beams with smart-structure technologies were reported. Among these, piezoelectric materials were the most rapidly developing materials used on sensors, actuators, and active control of flexible beam models [3–7]. Bergamini et al. [8] found that piezoelectric resonators can work as variable stiffness elements to control the band structure of a phononic crystal. Tzou and Gadre [9] proved the actuation effectiveness of a multilayered thin shell coupled with an active distributed polymeric piezoelectric polyvinylidene fluoride actuator both theoretically and experimentally.

Unlike the piezoelectricity, flexoelectricity is an intrinsic electromechanical coupling effect that does not rely on prepoling and, the aging problems encountered in piezoelectric dielectric after prepolarization could avoid in flexoelectric materials, thus, makes the flexoelectric dielectrics much more convenient for practical application. In principle, the flexoelectric effect could exist in most dielectrics; therefore, it is possible to discover or synthesize new flexoelectric materials with larger coupling coefficients for engineering application. With these advantages, flexoelectric materials show the potential as a substitution to piezoelectric materials to achieve precision actuation and active vibration control.

Contributed by the Technical Committee on Vibration and Sound of ASME for publication in the JOURNAL OF VIBRATION AND ACOUSTICS. Manuscript received May 4, 2017; final manuscript received January 5, 2018; published online February 23, 2018. Assoc. Editor: Mahmoud Hussein.

It is worth noting that there are two effects of the flexoelectricity: the direct flexoelectricity and the converse flexoelectricity. The direct flexoelectric effect describes the mechanism of a polarization response induced by the inhomogeneous mechanical fields (or strain gradients). Based on the direct flexoelectric effect, a direct curvature sensing measurement was demonstrated in a four-point bending test of a beam with bonded barium strontium titanate (BST) curvature sensors under different applied loads with low time-harmonic frequencies [10]. The flexoelectric barium strontium titanate cantilever was also used to design acceleration sensor by bonding the barium strontium titanate layer onto a steel substrate [11]. A new type of microphone using flexoelectric barium strontium titanate was developed [12]. Experiments of distributed sensing signals of beams suggested that distributed flexoelectric sensors were competent to provide the mode shape of strain gradients [13]. The converse flexoelectric effect describes the phenomenon of mechanical stress induced by the inhomogeneous polarization (or electric field gradient) [14–17]. The converse flexoelectric effect could apply to design flexoelectric actuators and controllers to actuate and control engineering structures if inhomogeneous electric field being established. In open literatures, one can find that asymmetric electrode configuration [18], trapezoid flexoelectric block [19], and comb electrode [20] were used to generate electric filed gradients. An atomic force microscope probe was also employed to generate inhomogeneous electric field to achieve beam vibration control [21].

In the current study, a line-electrode on the top surface of a flexoelectric beam together with a bottom surface electrode layer are used to achieve dynamic actuation and control of the cantilever beam by the converse flexoelectric effect. Both theoretical analysis and laboratory experiments are presented. To evaluate the control effects, key design parameters, e.g., line-electrode radius, flexoelectric beam thickness, and the line-electrode

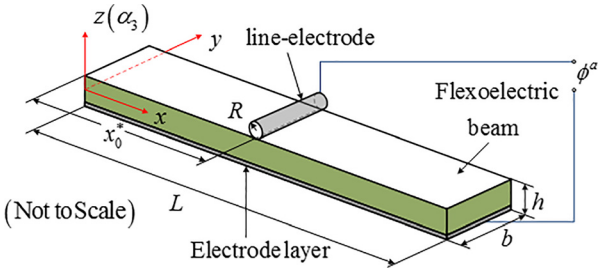

Fig. 1 Schematic diagram of flexoelectric beam model

position, are examined with respect to induced stresses, bending moments and dynamic tip displacements. Laboratory experiments conducted with different line-electrode locations are used to validate the theoretical predictions.

Mathematical Model

To actuate a flexoelectric cantilever beam, based on the *converse flexoelectric effect*, an inhomogeneous electric field is needed. A line-electrode is used to generate the electric field, which, in turn, actuates the flexoelectric beam. The flexoelectric cantilever beam and the corresponding electrodes are illustrated in Fig. 1, in which coordinates x and z, respectively, define the longitudinal and transverse directions. The length and width of the beam are denoted by L and b, respectively; R is the radius of the line-electrode and x_0^* is the position of the line-electrode on the top surface in the longitudinal direction.

A voltage ϕ^a is applied between the line-electrode placed on the top surface of the flexoelectric beam and the surface electrode layer below. For the beam considered here, both the length L and the width b are much larger than the beam thickness, i.e., $h \ll L$ and $h \ll b$, and the thickness is much larger than the radius of the line-electrode, i.e., $R \ll h$. Thus, the electric field between the line-electrode and the lower surface electrode can be assumed to be the same as the electric field between an infinite long cylindrical electrode and an infinite flat electrode. Note that the line-electrode cannot be regarded as infinitely thin, i.e., $R \neq 0$. In fact, the radius of the line-electrode, as discussed later, determines the actuation effect of the flexoelectric beam.

Flexoelectric Actuation Using Line-Electrodes. By regarding both the line-electrode and the lower surface electrode as infinite in the y direction, the model considered here can be reduced from a three-dimensional case to a two-dimensional electric field problem as illustrated in Fig. 2. The method of image charges (or the method of images) [22] is introduced to solve this electric field problem. When an actuation voltage is applied between the line-electrode and the lower surface electrode, the line-electrode is charged to Q per unit length, i.e., the line density on the line-electrode is Q. Assuming the charge on the line-electrode is positive and the potential of the lower surface electrode is zero (i.e., grounded), Q would induce a negative charge on the nearby surface of the lower electrode.

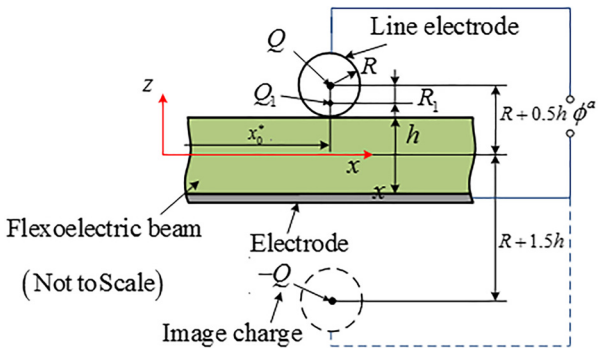

Fig. 2 Solution of the two-dimensional electric field problem with the method of images

From a mathematical perspective, the problem is to solve Poisson's equation in the $z \geq -(h/2)$ region with the boundary conditions of the potential on the surface of lower electrode being zero and the surface of line-electrode being equipotential. It can be guaranteed by the first uniqueness theorem that there is only one solution for the electric field. Thus, one could assume a solution which satisfies both Poisson's equation and the corresponding boundary conditions [22]. Then, such a solution would be a suitable solution. Introducing a line-electrode image charged with $-Q$ and placing its center at $(x_0^*, -(3h/2) - R)$, removing the lower electrode, one could prove that the electric field of this configuration, illustrated in Fig. 2, is identical to the original. Since the image line-electrode with $-Q$ appears, it would change the potential field on the surface of line-electrode. In another words, the charge on the surface of the line-electrode has to redistribute to maintain the line-electrode surface an equipotential surface. Such boundary condition can be satisfied by using the method of images for the line-electrode resulting in a charge $Q_1 = QR/(2R + 2h)$ located at $(x_0^*, (h/2) + R - R_1)$, where $R_1 = R^2/(2R + 2h)$ [22]. It can be proved that this approach would keep the surface of line-electrode equipotential. Note that the charge at the center of the line-electrode is reduced to $Q - Q_1$, due to the conservation of charges in the line-electrode meanwhile. While the appearance of the charge Q_1 would make the lower electrode plane nonequipotential until it images back in the plane. This process, as one may notice, continues infinitely and a sequence of image charges is obtained as Q_n. The recursion formula is given by $Q_n = (R/D_n)Q_{n-1}$, where $D_n \approx 2h + 2R$, and thus, $Q_n/Q_{n-1} \approx R/2(h + R)$. Recall that in this particular case $R \ll h$, thus $Q_n \ll Q_{n-1}$ and this indicates that the sequence of image charges decays rapidly. It is assumed here that only the first image charge inside the line-electrode is significant enough to induce flexoelectric actuation.

In summary, this problem is simplified to obtain the electric field generated by three lines with charges $Q - Q_1$, $-Q$, and Q_1, as depicted in Fig. 2. The expression of potential field ϕ is obtained first by substituting the potential field generated by these three line charges as [22]

$$\phi = -\frac{(Q - Q_1)}{2\pi\varepsilon}\ln\left(\sqrt{(x - x_0^*)^2 + \left(z - \frac{h}{2} - R\right)^2}\right) + \frac{Q}{2\pi\varepsilon}\ln\left(\sqrt{(x - x_0^*)^2 + \left(z + \frac{3h}{2} + R\right)^2}\right) - \frac{Q_1}{2\pi\varepsilon}\ln\left(\sqrt{(x - x_0^*)^2 + \left(z - \frac{h}{2} - R + \frac{R^2}{2R + 2h}\right)^2}\right) + C \tag{1}$$

where C is an arbitrary constant in the potential expression, since the zero potential point has not been clearly defined. To obtain the specific magnitude of potential field, the line charge density Q must be defined. Note that the potential difference between the lower electrode and the line-electrode must be the actuation voltage between them, i.e., ϕ^a. Thus, calculating the potential difference via Eq. (1) yields the relationship between the applied voltage and the unknown line density. Utilizing the expression of the potential field, substituting Q_1 by $QR/(2R + 2h)$ gives the potential difference

$$\phi^a = \phi(x,y)\Big|_{\text{lower electrode}}^{\text{line-electrode}} = \phi\left(x_0^*, \frac{h}{2}\right) - \phi\left(x_0^*, -\frac{h}{2}\right) = \frac{Q}{2\pi\varepsilon}\ln\left[\left(\frac{2h+R}{h+R}\right)\left(\frac{h+R}{R}\right)^{\frac{R+2h}{2R+2h}}\left(\frac{2(R+h)^2-R^2}{2R(R+h)-R^2}\right)^{\frac{R}{2R+2h}}\right] \tag{2}$$

From Eq. (2), one obtains the value of charge's line density. Substituting the expression of Q, i.e., solving from Eq. (2), into potential field yields the electric field distribution

$$\phi = \frac{-\phi^a}{\ln\left[\left(\frac{2h+R}{h+R}\right)\left(\frac{h+R}{R}\right)^{\frac{R+2h}{2R+2h}}\left(\frac{2(R+h)^2-R^2}{2R(R+h)-R^2}\right)^{\frac{R}{2R+2h}}\right]}\left\{\frac{R+2h}{2R+2h}\ln\left(\sqrt{(x-x_0^*)^2+\left(z-\frac{h}{2}-R\right)^2}\right)\right.$$
$$\left.-\ln\left(\sqrt{(x-x_0^*)^2+\left(z+\frac{3h}{2}+R\right)^2}\right)+\frac{R}{2R+2h}\ln\left(\sqrt{(x-x_0^*)^2+\left(z-\frac{h}{2}-R+\frac{R^2}{2R+2h}\right)^2}\right)\right\}+C \tag{3}$$

The magnitude of the potential field is determined by the summation of the three line charges shown in Fig. 2. Note that only the transverse electric field gradient is required to induce the flexoelectric stress and actuation in the cantilever beam [23]. The transverse electric field can be obtained by taking the partial derivative in the transverse direction of the potential expression as

$$E_z(x,z) = -\frac{\partial\phi}{\partial z} = \frac{\phi^a}{\ln\left[\left(\frac{2h+R}{h+R}\right)\left(\frac{h+R}{R}\right)^{\frac{R+2h}{2R+2h}}\left(\frac{2(R+h)^2-R^2}{2R(R+h)-R^2}\right)^{\frac{R}{2R+2h}}\right]}$$
$$\left\{\frac{\frac{R+2h}{2R+2h}\left(z-\frac{h}{2}-R\right)}{\left((x-x_0^*)^2+\left(z-\frac{h}{2}-R\right)^2\right)}-\frac{\left(z+\frac{3h}{2}+R\right)}{\left((x-x_0^*)^2+\left(z+\frac{3h}{2}+R\right)^2\right)}+\frac{\frac{R}{2R+2h}\left(z-\frac{h}{2}-R+\frac{R^2}{2R+2h}\right)}{\left((x-x_0^*)^2+\left(z-\frac{h}{2}-R+\frac{R^2}{2R+2h}\right)^2\right)}\right\} \tag{4}$$

With the transverse electric field induced by the line-electrode, one derives the longitudinal stress induced by the electric field gradient defined by the converse flexoelectric equation

$$T_{xx}^a = \pi_{12}\frac{\partial E_z}{\partial z} \tag{5}$$

where T_{xx}^a indicates the longitudinal stress induced by the inhomogeneous electric field generated by the line-electrode and the superscript a denotes the actuator term (i.e., the electrodes/flexoelectric beam system in this case); π_{12} is a flexoelectric constant. With the induced stress expression, the flexoelectric actuation membrane force can be obtained by calculating the overall stress contribution along the transverse direction and it can be expressed as

$$N_{xx}^a = \int_{-\frac{h}{2}}^{\frac{h}{2}} T_{xx}^a\, dz \tag{6}$$

where N_{xx}^a is the membrane force induced by the actuator. The bending control moment M_{xx}^a induced by the actuator can also be calculated by integrating the product of the actuation stress and the corresponding moment arm, i.e., the distance from the beam's neutral layer to a local point

$$M_{xx}^a = \int_{-\frac{h}{2}}^{\frac{h}{2}} T_{xx}^a z\, dz \tag{7}$$

With the specific expression of actuation membrane force and bending control moment induced by the line-electrode, the actuation effect based on flexoelectricity is discussed later.

Dynamics of Cantilever Beam. The dynamic equation of the cantilever beam free from external force can be deducted from the generic double-curvature shell as [24]

$$\rho A\ddot{u}_3 + YI\frac{\partial^4 u_3}{\partial x^4} = b\frac{\partial^2 M_{xx}^a}{\partial x^2} \tag{8}$$

where u_3 is the transverse displacement, $A = bh$ is the cross section area, I is the area moment of the cross section which is defined as $I = bh^3/12$, Y is the Young's modulus, ρ is the mass density of the beam, and M_{xx}^a is, as defined previously, the flexoelectric bending control moment. The modal expansion method is introduced here to describe the vibration of the cantilever beam. The dynamic transverse displacement can be written as the summation of every modal participation factor multiplied by its corresponding mode shape function as

$$u_3 = \sum_{k=1}^{\infty}\eta_k(t)U_{3k}(x) \tag{9}$$

where U_{3k} is the transverse mode shape function, subscribe k denotes the mode number, and η_k is the corresponding modal participation factor. U_{3k} denotes the spatial distribution and η_k denotes the temporal contribution of each mode. For a cantilever elastic beam, the mode shape function is defined by

$$U_{3k}(x) = C_k\left[C(\lambda_k x) - \frac{A(\lambda_k L)}{B(\lambda_k L)}D(\lambda_k x)\right] \tag{10}$$

Table 1 Parameters and properties of the model

Properties	Values
Beam length, L (m)	0.100
Beam width, b (m)	0.010
Beam thickness, h(m)	0.001
Young's modulus of beam, Y(GPa)	153
Line-electrode radius, R (μm)	100
Actuation voltage, ϕ^a (V)	1
Beam mass density, ρ (kg/m^3)	5650
Flexoelectric constant, π_{12} (μC/m)	100

where $A(\lambda_k x)=(\cosh\lambda_k x+\cos\lambda_k x)$, $B(\lambda_k x)=(\sinh\lambda_k x+\sin\lambda_k x)$, $C(\lambda_k x)=(\cosh\lambda_k x-\cos\lambda_k x)$, and $D(\lambda_k x)=(\sinh\lambda_k x-\sin\lambda_k x)$, λ_k is the eigenvalue or the kth root of the characteristic equation $\cosh\lambda_k x+\cos\lambda_k x=0$, and the coefficient C_k is defined as $C_k=(1/\lambda_k^2)(d^2U_{3k}/dx^2)(0)$. The first five roots of the characteristic equation are $\lambda_k L=1.875,4.694,7.855,10.996,14.137,(k=1\ldots5)$. Note that the magnitude C_k is a function of the excitation and thus arbitrary as far as the mode shape is considered.

To obtain the vibration displacement of the beam u_3, one should also determine the modal participation factor η_k of each mode. When the actuation voltage applied between the line-electrode and the lower surface electrode is harmonic, i.e., $\phi^a(t)=\phi^a e^{j\omega t}$, the actuation force on the beam varies harmonically with time and the response is also harmonic at steady-state. Substituting the modal expansion expression into the dynamics equation of the beam, utilizing the orthogonality of mode shape functions, one derives the modal equation

$$\ddot{\eta}_k+2\zeta_k\omega_k\dot{\eta}_k+\omega_k^2\eta_k=\hat{F}_k^* e^{j\omega t} \tag{11}$$

where ω_k denotes the kth mode natural frequency and it is determined by the characteristics of the cantilever beam as $\omega_k=\lambda_k^2\sqrt{YI/\rho A}$, ζ_k is the modal damping ratio which is related to natural frequency ω_k and equivalent damping constant c as $\zeta_k=c/(2\rho h\omega_k)$, and $\hat{F}_k^*$ denotes the magnitude of the kth modal force, which is induced only by the actuator (line-electrode) here and it can be expressed as [24]

$$\hat{F}_k^*=\frac{1}{\rho h N_k}\int_0^L -\left(\frac{\partial^2 M_{xx}^a}{\partial x^2}\right)U_{3k}dx \tag{12}$$

where $N_k=\int_0^L U_{3k}^2dx$. With the magnitude of the modal force, the modal response (modal participation factor η_k) can be obtained by solving the modal equation, i.e., Eq. (11), as

$$\eta_k(t)=\frac{\hat{F}_k^*}{(\omega_k^2-\omega^2)+2j\zeta_k\omega_k\omega}e^{j\omega t}=\frac{\hat{F}_k^*}{\omega_k^2\sqrt{\left(1-\frac{\omega^2}{\omega_k^2}\right)^2+4\zeta_k^2\left(\frac{\omega}{\omega_k}\right)^2}}e^{j(\omega t-\varphi^*)} \tag{13}$$

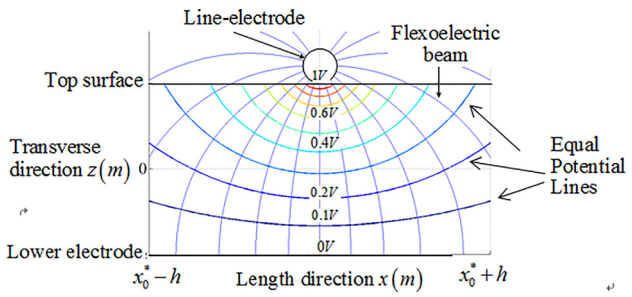

Fig. 3 Spatial distribution of the potential field and the electric field

where φ^* is the phase angle defined as $\varphi^*=\arctan\left(2\zeta_k(\omega/\omega_k)/1-(\omega/\omega_k)^2\right)$. Considering the modal expanding expression, mode shape functions and the expression of modal participation factors, one can derive the transverse vibration displacement $u_3(x,t)$ (i.e., the flexoelectric induced controllable deflection) of the cantilever beam

$$\begin{aligned}u_3(x,t)&=\sum_{k=1}^{\infty}\eta_k(t)U_{3k}(x)\\&=\sum_{k=1}^{\infty}\frac{\hat{F}_k^*}{\omega_k^2\sqrt{\left(1-\frac{\omega^2}{\omega_k^2}\right)^2+4\zeta_k^2\left(\frac{\omega}{\omega_k}\right)^2}}U_{3k}(x)\,e^{j(\omega t-\varphi^*)}\\&=\sum_{k=1}^{\infty}\frac{\left[\int_0^L-\left(\frac{\partial^2 M_{xx}^a}{\partial x^2}\right)U_{3k}dx\right]U_{3k}(x)e^{j(\omega t-\varphi^*)}}{\rho h N_k\omega_k^2\sqrt{\left(1-\frac{\omega^2}{\omega_k^2}\right)+4\zeta_k^2\left(\frac{\omega}{\omega_k}\right)^2}}\end{aligned} \tag{14}$$

The transverse vibration of the cantilever beam is affected by the flexoelectric bending moment induced by the actuation only. Given an actuation voltage, the induced control moment can be calculated, i.e., Eq. (7). Furthermore, dynamic actuation and vibration behavior of the beam under the applied voltages can be evaluated, i.e., Eq. (14). With the parameters listed in Table 1, actuation effects of the line-electrode actuator are evaluated and discussed next.

Case Studies

Spatial characteristics of the electric field induced by the line-electrode and the resulting stress are analyzed first, followed by evaluations of the flexoelectric induced moment and harmonic actuation effects in case studies.

Electric Field. When an actuation voltage ϕ^a is applied between the line-electrode and the lower surface electrode, the spatial distribution of the potential and the electric field induced by the line-electrode is illustrated in Fig. 3.

In Fig. 3, the lines radiate from the line-electrode are the electric field lines; the lines perpendicular to the fields (and somehow parallel to the surface of the line-electrode) are the equal potential lines. Note that Fig. 3 is drawn in a small region (i.e., $2h$ in width,

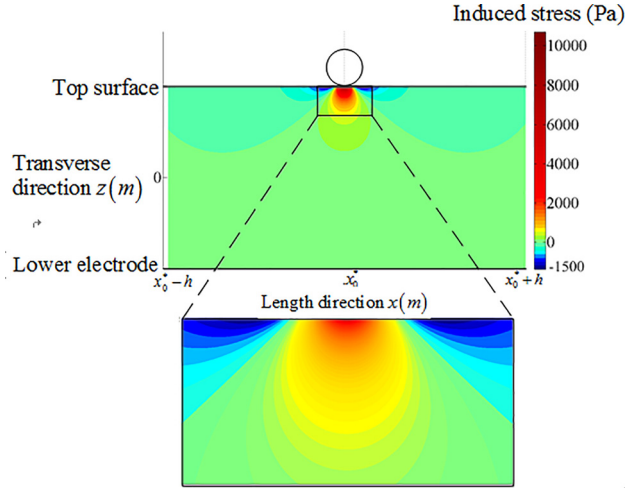

Fig. 4 Spatial distribution of induced longitudinal normal stress

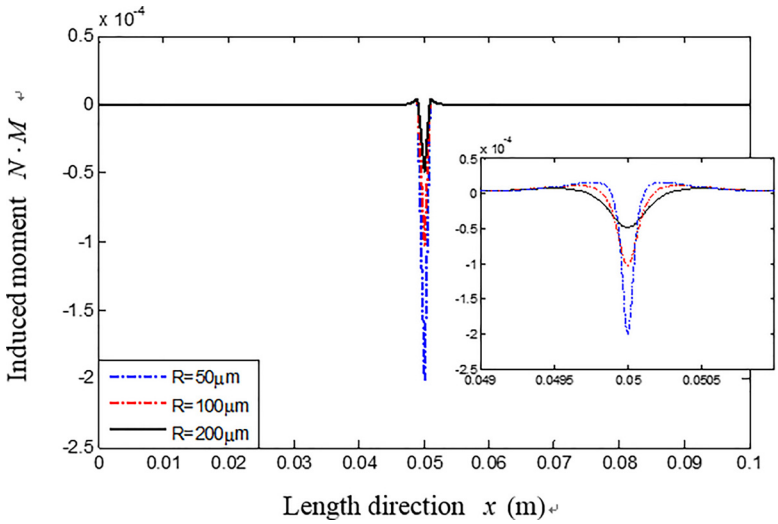

Fig. 5 Longitudinal distribution of the induced moment under different line-electrode radius

h in height) closed to the location of the line-electrode, since the local electric gradient is relatively large as compared with the region far away from the line-electrode. The potential of the electric field, as shown in Fig. 3, is relatively high in the region near the line-electrode and decays rapidly with the distance away from the line-electrode. The electric field lines, closed with each other in the region around the line-electrode, separate from each other as they move away from the line-electrode. This indicates that the electric field strength near the line-electrode is larger and smaller when away. Thus, the electric gradient is generated in the transverse direction, which, in turn, as demonstrated by the converse flexoelectric effect, induces the stresses inside the flexoelectric cantilever beam.

Flexoelectric Induced Stresses. The relationship between the longitudinal induced stress in the flexoelectric beam and the transverse electric field is given by the stress expression Eq. (5), i.e., the induced stress is proportional to the gradient of the transverse electric field. According to the distribution of the electric field induced by the line-electrode, the spatial distribution of the magnitude of induced longitudinal normal stress is plotted in Fig. 4.

Figure 4 indicates that the stress in the area underneath the line-electrode is extremely large and it decreases to zero as it moves away from the line-electrode. To have a better understanding of the stress distribution, the stress distribution close to the line-electrode is enlarged below in Fig. 4. One may observe that the stress in the region underneath the line-electrode is positive and the stress becomes negative in a small area next to the positive region. Such phenomenon can be explained by analyzing the electric field plot, i.e., Fig. 3. For the region on the left of the line-electrode, although the electric field strength is relatively strong, its direction is almost horizontal. Thus, the transverse electric field can be relatively small in that region; for the region right under it, although the electric field strength is weaker, the angle between the electric field with the horizontal line, i.e., slope, is larger. Thus, the transverse electric field strength can be greater than the former one. Under such circumstance, the strength of the transverse electric field drops in the positive transverse direction. In another words, the value of the gradient of the transverse electric

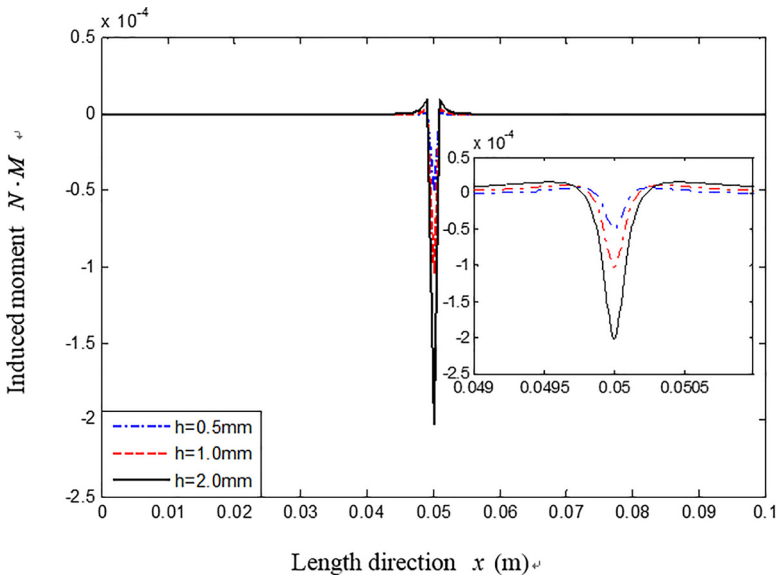

Fig. 6 Longitude distribution of the induced moment under different beam thickness

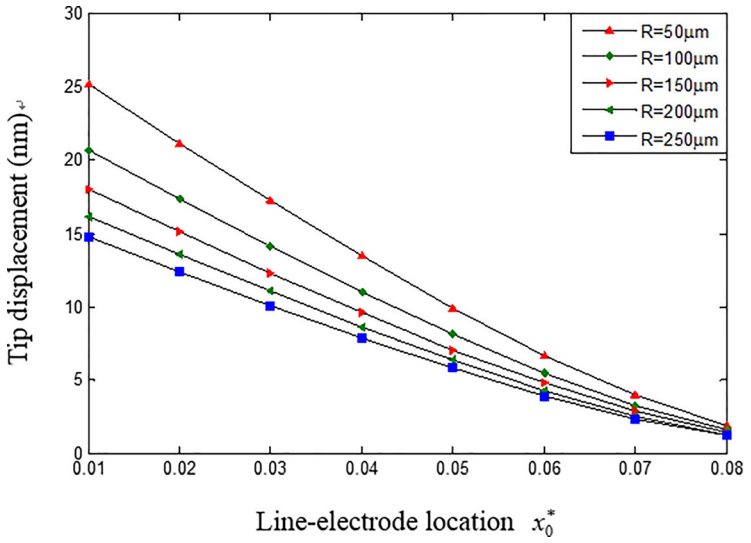

Fig. 7 Tip displacement with the line-electrode location under different line-electrode radius

field is negative, which leads to the stress there being negative in the region to the left of the line-electrode [25]. The same physics appears on the right side of the line-electrode, and thus, it forms two negative-stress regions on both sides on the line-electrode. The negative-stress magnitude, as shown in Fig. 4, is much less than the positive one in both areas. Hence, the contribution of the positive stress to the overall actuation effect is dominant as compared with the negative ones. However, the appearance of the negative stresses would introduce intriguing actuation characteristics when the induced control moments are considered.

Flexoelectric Induced Actuation Moments. Recall the displacement induced by the actuation of line-electrode, i.e., Eq. (14), the longitudinal distribution of the induced moment determines the actuation effect of the actuator (i.e., electrodes and the beam). The induced actuation moment can be evaluated by integrating the stress multiplied by the moment arm, as demonstrated in Eq. (7). Variation of the longitudinal distribution of the induced moment with two design parameters, i.e., the line-electrode radius and the flexoelectric beam thickness, is evaluated here. The distributions of induced moments are plotted with respect to line-electrode radius of 50 μm, 100 μm, and 200 μm in Fig. 5.

Note that the line-electrode is placed at $x_0^* = 0.05$m and the moment distribution is plotted in a region close to the electrode, i.e., from $x_0^* - h$ to $x_0^* + h$. As shown in Fig. 5, the magnitude of induced moment reaches a maximum at the point underneath the line-electrode and decays rapidly away from the electrode, i.e., a spike is formed at the line-electrode location. As the radius of the line-electrode decreases, the spike becomes shaper and the maximal absolute value of the induced moment increases. This is reasonable because as the electrode is relatively thin, the induced electric field is rather concentrated. Thus, the induced stress near the line-electrode increases and the stress decays faster in the longitudinal direction, which leads to the longitudinal distribution of the induced moment being sharper as illustrated in Fig. 5. Note that the maximum induced moment is negative in the region underneath the line-electrode. However, positive induced

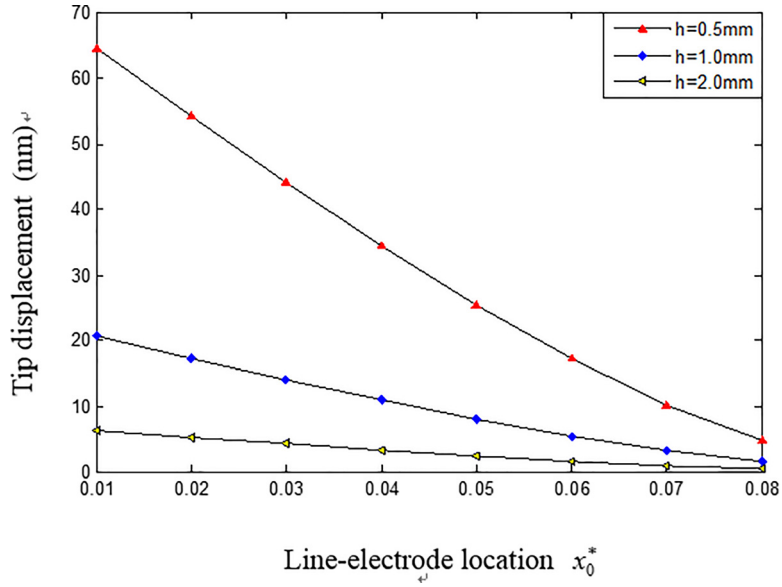

Fig. 8 Tip displacement with the line-electrode location under different beam thickness

moments are observed away from the line-electrode location. The appearance of the positive induced moments whose direction different from the moment underneath the line-electrode can be explained by the stress distribution inside the flexoelectric beam. Recall that for the region near the top surface of the beam but away from the line-electrode, as shown in Fig. 4, the induced stress is of opposite direction compared with the stress in the region underneath the electrode, i.e., if the stress right under the electrode is considered pulling, the stress away from it will be pushing [25]. Note that the stress contributes to the magnitude of induced moments directly. Thus, it is reasonable that the longitudinal distribution of the induced moment can be of different directions. This distribution of induced moment means that under the actuation of the line-electrode the beam is bend to one direction at the point where line-electrode is placed, while bend to another direction in outer regions.

Line-electrode radius influences both the magnitude and the distribution of the induced moments. Another parameter, the thickness of the flexoelectric beam, is also evaluated here. Figure 6 illustrates the distributions of the induced moments with respect to beam thickness of 0.5 mm, 1.0 mm, and 2.0 mm.

Figure 6 reveals that although the magnitude of the induced moment increases with the beam thickness, their spatial distribution patterns are similar, i.e., negative to positive regions. Recall the induced stress distribution in Fig. 4; the stress is much larger near the top surface and it decreases when moving away from the contact point. Accordingly, the upper part of the flexoelectric beam is the major component contributing to the actuating bending moment and the induced moment can be approximately calculated by multiplying the induced membrane force with its moment arm. Since the area generating major membrane force is closed to the top surface and away from the neutral layer, both the magnitude and the distribution of the membrane force would not change with the beam thickness. However, the moment arm increases as the thickness increases and this leads to the induced moment increasing with the thickness. Because the moment arm remains constant along the longitudinal beam direction, the distribution of the induced moment does not change since the membrane force remained unchanged. The actuation effect, defined as the induced tip displacement of the cantilever beam, is evaluated next.

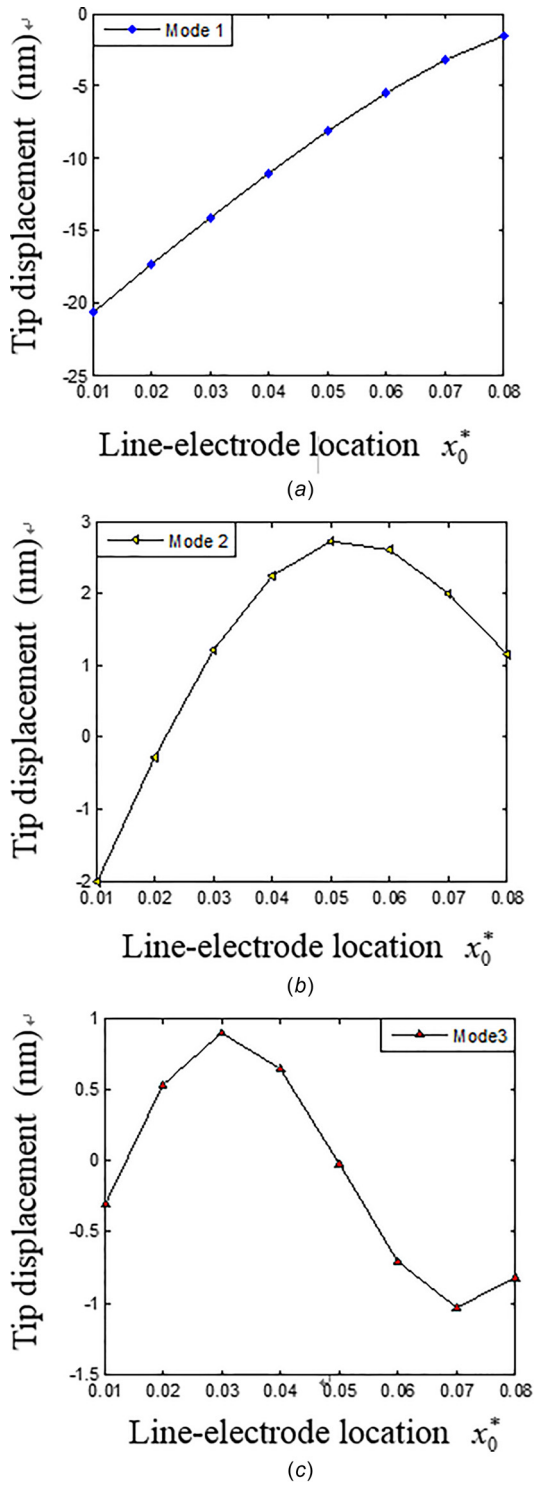

Fig. 9 Tip displacement with the line-electrode location under (*a*) mode 1, (*b*) mode 2, and (*c*) mode 3

Flexoelectric Actuation Effects. With the investigation of flexoelectric actuation characteristics previously, analysis and evaluation of the flexoelectric actuation effect (or induced controllable deflections) are much easier. When a harmonic actuation voltage is applied between the line-electrode and the lower surface electrode, the response of the cantilever beam is also harmonic. Since the fundamental mode usually dominates the beam oscillation, the excitation frequency is set to be the first natural frequency of the cantilever beam first and the induced tip controllable displacement is evaluated with the harmonic response expression, i.e., Eq. (14). The same as the earlier induced moment study, influences of the line-electrode radius and the beam thickness are evaluated, followed by natural modal effects. Particularly, the flexoelectric beam is divided into nine parts with eight lines, the line-electrode is placed on those lines one by one and the corresponding actuation effect is obtained. The tip displacements are plotted when the line-electrode is placed at eight different points on the beam with respect to line-electrode radius of 50 μm, 100 μm, 150 μm, 200 μm, and 250 μm in Fig. 7. The electrode location are chosen from $x_0^* = 0.01$ to $x_0^* = 0.08$. The rest parameters of the system are the same as shown in Table 1.

For a given line-electrode radius, as indicated in Fig. 7, the actuation effect or flexoelectric induced displacement reduces as the line-electrode moving from the fixed end toward the beam tip. Note that such decay is determined by the characteristics of the first mode shape function. As the electrode radius enlarges, the tip displacement decreases at each position of the line-electrode. This can be explained by the longitudinal distribution of the induced moment under the actuation of different radius of line-electrodes. A thinner line-electrode enhances the electric field gradient consequently resulting in a larger induced tip displacement and actuation effect.

Another design parameter, the effect of the flexoelectric beam thickness is evaluated. Again, the line-electrode is positioned at the eight locations successively. The induced tip displacements are evaluated when the line-electrode is placed from 0.01 m to 0.08 m with respect to beam thicknesses of 0.5 mm, 1.0 mm, and

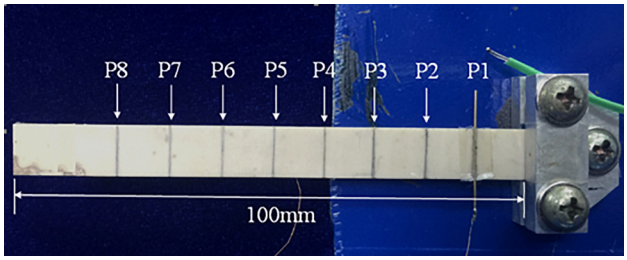

Fig. 10 The flexoelectric beam and its eight line-electrodes

Table 2 Geometrical and material parameters of the flexoelectric beam

Properties	Values
Beam length, L (m)	0.1
Beam width, b (m)	0.0096
Beam thickness, h(m)	0.00101
Young's modulus of beam, Y (GPa)	150.8
Damping ratio, ζ	0.0099
Actuation voltage, ϕ^a (V)	200
Beam mass density, ρ(kg/m^3)	5636
Flexoelectric constant, π_{12} (μC/m)	97

2.0 mm in Fig. 8. Other parameters of the system are the same as presented in Table 1.

Similar to Fig. 7, given a beam thickness, the flexoelectric induced tip displacement decays as the line-electrode moving toward the free end of the beam. For each line-electrode position, the relationship between the beam thickness and the induced tip displacement is approximately negatively quadric. Recall that in the analysis of induced moment under different beam thickness, as the thickness grows the moment enhanced due to an increase of moment arm. Because the moment arm varies with beam thickness nearly linearly, the magnitude of actuation force increases quasi-linearly with the beam thickness. Furthermore, as the beam becomes thicker, there is a cubic growth of bending stiffness, which means the beam becomes much harder to actuate. Thus, the relationship between the actuation effect and the beam thickness, as demonstrated earlier, is quasi-quadric.

For the last case here, the actuation effects induced by line-electrodes placed at different locations of the beam from 0.01 m to 0.08 m under the excitation frequencies of the first, second, and third natural modes are evaluated, respectively. Recall that for the first natural frequency, the induced tip displacement reduces as the line-electrode approaching the free end. While such monotonic decreasing is related to the first mode shape function of the cantilever beam, the actuation characteristic of other modes may well be different comparing with the first one. The induced tip displacements at different line-electrode locations are plotted with respect to the first, second, and third natural frequencies in Fig. 9.

As shown in Fig. 9, the optimal actuation position for the second mode is 0.05 m and for the third mode is 0.07 m, which are different to the first mode. One may notice that, just as the first mode, Fig. 9(*b*) resembles the second mode shape and Fig. 9(*c*) resembles the third mode shape of cantilever beam. To validate the analyses and theoretical predictions, a flexoelectric physical model is tested and its experimental data are compared with analytical results presented next.

Experiment Validation. A physical flexoelectric cantilever beam is prepared with a line-electrode on the top surface and an electrode layer on the bottom surface. Flexoelectric samples used in experiments are slender BST bars supplied by Shanghai Institute of Ceramics, Chinese Academy of Science. To generate an inhomogeneous electric field, the BST beam, as described earlier, was fully deposited with conductive electrodes on the bottom surface and a thin copper wire is applied as a line-electrode fixed on the top surface of the beam, as shown in Fig. 10. Eight lines, denoted by P1, P2, …, P8, were drawn on the top surface of the beam and serve as reference locations of the line-electrode moving from one end to the other, i.e., P1 to P8, during laboratory experiments. One end of the beam is fixed on a solid fixture, whereas the other end is free. The tip displacement is measured at the free end of the cantilever beam (left end of Fig. 10) when the actuation line-electrode moves from P1 to P8, respectively. Note that since the mass of the copper wire used here is much smaller than that of BST beam (i.e., around 0.5% to 1% of the beam mass), the influence of the weight of copper wire electrode on the vibration of the flexoelectric beam is neglected.

A harmonic actuation voltage is needed to actuate or excite the flexoelectric beam and it is generated by a function generator (Hewlett-Packard 33120A) and amplified by a power amplifier (Trek Model PZD700A). To evaluate the actuation effect of the actuator, the tip displacement of the cantilever beam is measured by a Laser Doppler Vibrometer (Sunny LV-S01, abbreviated as LDV) and the signal is collected by a data acquisition and analysis

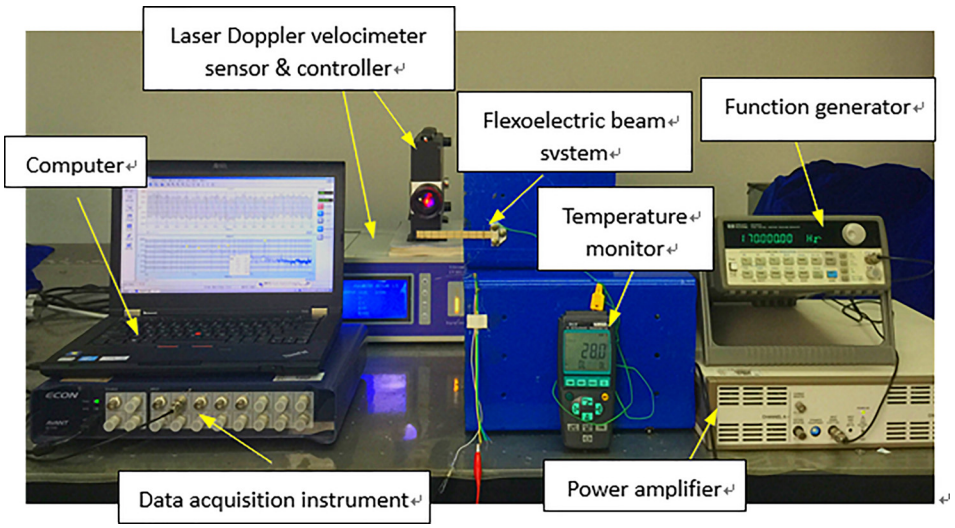

Fig. 11 Experimental setup for evaluating flexoelectric actuation effect

instrument (ECON AVANT MI-7016). The experimental setup is illustrated in Fig. 11.

The velocity data of the beam's tip vibration is integrated by a computer to obtain the displacement information. Earlier experimental studies indicated that the temperature fluctuation influences BST proprieties, i.e., relative permittivity, loss tangent, etc. [13]. In order to minimize temperature effects, the laboratory temperature was kept at 28 °C when conducting experiments. In the experiment, a BST cantilever beam with length 109.64 mm, width 9.6 mm, thickness 1.01 mm is used. Since one end was clumped on the fixture, after subtracting the clamped part, the overhung length of the flexoelectric beam is 100 mm, which is consistent with the former theoretical model. Detailed geometrical parameters and material properties are given in Table 2.

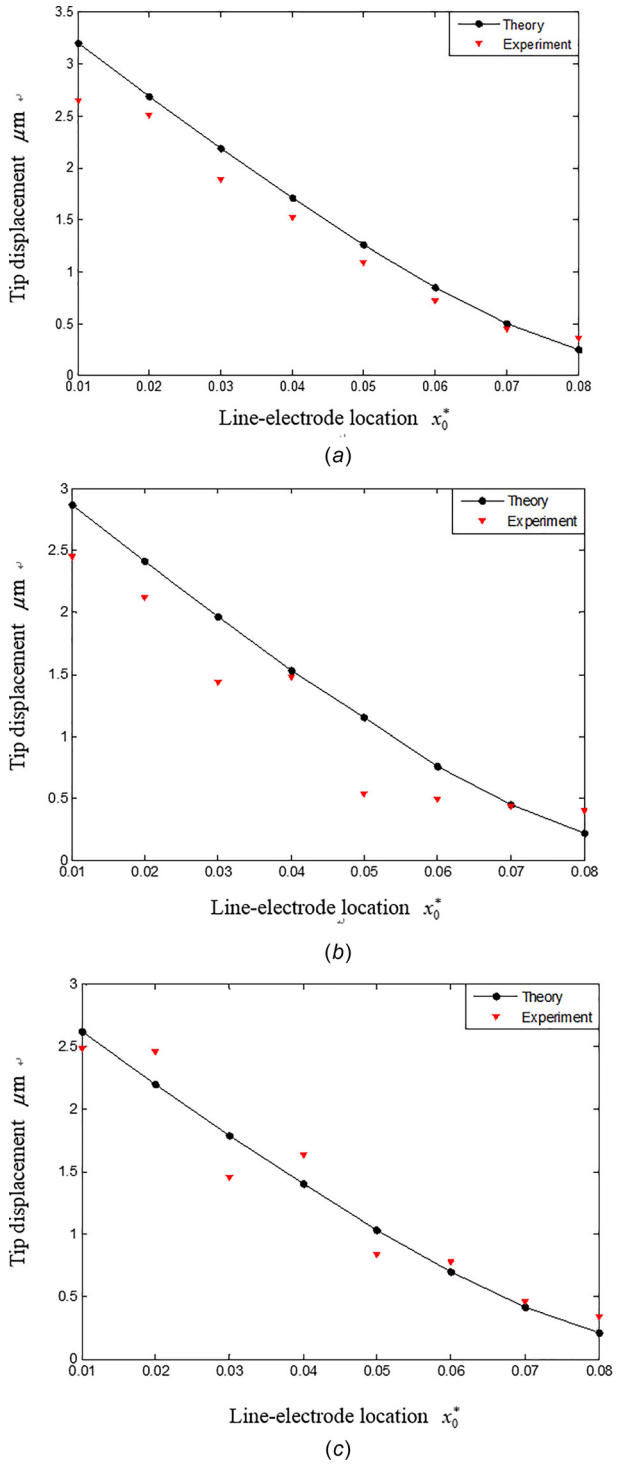

Fig. 12 Measured and predicted data of tip displacements with (*a*) $R = 150\ \mu$m, (*b*) $R = 200\ \mu$m, and (*c*) $R = 250\ \mu$m

Tip (i.e., free-end) displacement of the beam subjected to line-electrode harmonic excitations is measured and the data are compared with theoretical analysis. All the experimental data presented below was chosen as an average of five repeated experiments on the same beam to guarantee accuracy. Again, since the first mode is the dominating mode, only the first mode actuation characteristics are evaluated and compared. Figure 12 illustrates the first mode flexoelectric actuation effects of controllable deflections with respect to eight line-electrode positions from P1 to P8 and three line-electrode radius of 150 μm, i.e., Fig. 12(*a*), 200 μm, i.e., Fig. 12(*b*), and 250 μm, i.e., Fig. 12(*c*).

In general, the experimental data follows well with respect to theoretical predictions in Fig. 12, but fluctuates at some points, like P3, P5 in Fig. 12(*b*). The difference of P5 between the theoretical prediction and experiment data is about 60%, the rest data are well within $\pm 20\%$ of the theoretical predictions. The errors could be induced by material inhomogeneity of the beam sample, LDV measurement deviations or unstable floors since the induced displacement is in micrometer. Besides, the metal fixture, as a good conductor, would influence the electric field distribution generated by the line-electrode and lower surface electrode, which can also impact the measurement accuracies. A second thicker, i.e., length 109.68 mm, width 10.06 mm and thickness 2.03 mm was used to repeat experiment by following identical experimental procedures, and smaller tip displacements were observed. It is because of increasing beam thickness, the induced electric field gradient decreases.

Conclusions

Dynamic actuation characteristics and vibration control of a flexoelectric cantilever beam with the converse flexoelectricity were evaluated theoretically and experimentally in this study. A line-electrode was used to generate the electric field gradient so that internal stresses and then actuation moments were induced. Flexoelectric induced modal tip displacements or controllable deflections of the cantilever beam were evaluated at resonance. Theoretical and experimental results with respect to design parameters were investigated and compared. Since the fundamental mode usually dominates the beam oscillation, the first natural frequency was used as the excitation frequency of the input signal. Analytical results showed that thinner-radius line-electrode and thinner flexoelectric beam leads to larger control effects. Besides, the line-electrode location also had great influence on the control effects, which was proved analytically and experimentally. Moving the line-electrode from the fixed end of the free end, the induced tip displacement decreased. The analytical results generally agreed well with the experimental data collected from laboratory experiments. Thus, this study would provide fundamental insights of flexoelectric actuation and possible design guidelines in engineering applications.

Funding Data

- Natural Science Foundation of China (Grant Nos. 11702130, 11472241, and 11172262).
- Natural Science Foundation of Jiangsu Province (Grant No. BK20170773).
- Nanjing University of Aeronautics and Astronautics Foundation (Grant No. NUAA-NP2016203).
- State Key Laboratory of Mechanics and Control of Mechanical Structures (Grant No. NUAA-MCMS-0516G01).

References

[1] Soedel, W., 2004, *Vibrations of Shells and Plates—Revised and Expanded*, 3rd ed., Marcel Dekker, New York.

[2] Qatu, M.-S. K., 2004, *Vibration of Laminated Shells and Plates*, Elsevier, San Diego, CA.
[3] Tzou, H. S., and Ye, R., 1994, "Piezothermoelasticity and Precision Control of Piezoelectric Systems: Theory and Finite Element Analysis," ASME J. Vib. Acoust., **116**(4), pp. 489–495.
[4] Tzou, H., and Hollkamp, J., 1999, "Collocated Independent Modal Control With Self-Sensing Orthogonal Piezoelectric Actuators—Theory and Experiment," Smart Mater. Struct., **3**(3), pp. 277–284.
[5] Bao, Y., Tzou, H. S., and Venkayya, V. B., 1998, "Analysis of Non-Linear Piezothermoelastic Laminated Beams With Electric and Temperature Effects," J. Sound Vib., **209**(3), pp. 505–518.
[6] Wang, D. W., Tzou, H. S., and Lee, H. J., 2004, "Control of Nonlinear Electro/Elastic Beam and Plate Systems (Finite Element Formulation and Analysis)," ASME J. Vib. Acoust., **126**(1), pp. 63–70.
[7] Tzou, H. S., and Ye, R., 1996, "Analysis of Piezoelastic Structures With Laminated Piezoelectric Triangle Shell Elements," AIAA J., **34**(1), pp. 110–115.
[8] Bergamini, A., Delpero, T., De, S. L., Di, L. L., Ruzzene, M., and Ermanni, P., 2014, "Phononic Crystal With Adaptive Connectivity," Adv. Mater., **26**(9), pp. 1343–1347.
[9] Tzou, H. S., and Gadre, M., 1989, "Theoretical Analysis of a Multi-Layered Thin Shell Coupled With Piezoelectric Shell Actuators for Distributed Vibration Controls," J. Sound Vib., **132**(3), pp. 433–450.
[10] Yan, X., Huang, W., Ryung Kwon, S., Yang, S., Jiang, X., and Yuan, F. G., 2013, "A Sensor for the Direct Measurement of Curvature Based on Flexoelectricity," Smart Mater. Struct., **22**(8), pp. 1–8.
[11] Huang, W., Kwon, S. R., Zhang, S., Yuan, F. G., and Jiang, X., 2014, "A Trapezoidal Flexoelectric Accelerometer," J. Intell. Mater. Syst. Struct., **25**(3), pp. 271–277.
[12] Kwon, S. R., Zhang, S., Yuan, F. G., and Jiang, X., 2014, "A New Type of Microphone Using Flexoelectric Barium Strontium Titanate," Proc. SPIE, **9062**, pp. 2978–2982.
[13] Hu, S. D., Li, H., and Tzou, H. S., 2015, "Distributed Flexoelectric Structural Sensing: Theory and Experiment," J. Sound Vib., **348**, pp. 126–136.
[14] Fu, J. Y., Zhu, W., Li, N., and Smith, N. B., 2007, "Gradient Scaling Phenomenon in Microsize Flexoelectric Piezoelectric Composites," Appl. Phys. Lett., **91**(18), p. 182910.
[15] Kogan, S. M., 1964, "Piezoelectric Effect During Inhomogeneous Deformation and Acoustic Scattering of Carriers in Crystals," Sov. Phys.-Solid States, **5**(10), pp. 2069–2070.
[16] Tagantsev, A. K., 1986, "Piezoelectricity and Flexoelectricity in Crystalline Dielectrics," Phys. Rev. B, **34**(8), pp. 5883–5889.
[17] Todorov, A. T., Petrov, A. G., and Fendler, J. H., 1994, "First Observation of the Converse Flexoelectric Effect in Bilayer Lipid Membranes," J. Phys. Chem., **98**(12), pp. 3076–3079.
[18] Baskaran, S., Thiruvannamalai, S., Heo, H., Lee, H. J., Francis, S. M., Ramachandran, N., and Fu, J. Y., 2010, "Converse Piezoelectric Responses in Non-piezoelectric Materials Implemented Via Asymmetric Configurations of Electrodes," J. Appl. Phys., **108**(6), p. 064114.
[19] Fu, J. Y., Zhu, W., Li, N., and Cross, L. E., 2006, "Experimental Studies of the Converse Flexoelectric Effect Induced by Inhomogeneous Electric Field in a Barium Strontium Titanate Composition," J. Appl. Phys., **100**(2), pp. 6394–6401.
[20] Shen, Z., and Chen, W., 2012, "Converse Flexoelectric Effect in Comb Electrode Piezoelectric Microbeam," Phys. Lett. A, **376**(19), pp. 1661–1663.
[21] Hu, S. D., Li, H., and Tzou, H. S., 2011, "Static Nano-Control of Cantilever Beams Using the Inverse Flexoelectric Effect," ASME Paper No. IMECE2011-65123.
[22] Griffiths, D. J., 1999, *Introduction to Electrodynamics*, 3rd ed., Prentice Hall, Upper Saddle River, NJ.
[23] Hu, S. D., Li, H., and Tzou, H. S., 2014, "Comparison of Flexoelectric and Piezoelectric Dynamic Signal Responses on Flexible Rings," J. Intell. Mater. Syst. Struct., **25**(7), pp. 832–844.
[24] Tzou, H. S., 1993, *Piezoelectric Shells: Distributed Sensing and Control*, Kluwer Academic Publishers, London.
[25] Tzou, H., Deng, B., and Huiyu, L. I., 2017, "Flexoelectric Actuation and Vibration Control of Ring Shells," ASME J. Vib. Acoust., **139**(3), p. 031014.